The role of particle size and other properties on silo discharge behaviour of chipped wood biomass

Hamid Salehi [a,c,d,*], Jessica Gard Timmerfors [b,1], Hajar Hajmohammadi [e], Vivek Garg [c], Robert J. Berry [c], Diego Barletta [d], Massimo Poletto [d], Leif J. Jönsson [b], Michael S.A. Bradley [c], Sylvia H. Larsson [a,1]

[a] *Swedish University of Agricultural Sciences, Biomass Technology Centre, Department of Forest Biomaterials and Technology, Skogsmarksgränd, SE-90183 Umeå, Sweden*
[b] *Department of Chemistry, Umeå University, SE-901 87 Umeå, Sweden*
[c] *Wolfson Centre for Bulk Solids Handling Technology, Faculty of Engineering & Science, University of Greenwich, Central Avenue, Chatham ME4 4TB, United Kingdom*
[d] *Department of Industrial Engineering, University of Salerno, Via Giovanni Paolo II, 84084 Fisciano, SA, Italy*
[e] *Institutes of Science, Queen Mary University of London, E1 2AB London, United Kingdom*

HIGHLIGHTS

- A novel drum chipper was utilised to generate wood chips from several tree species.
- Wood chips' flow characteristics were tested with a biomass-specific shear tester.
- Critical arching conditions were experimentally measured with a wedge-shaped hopper.
- Based on statistical model, chips property cause Jenike and experiment disparities.

GRAPHICAL ABSTRACT
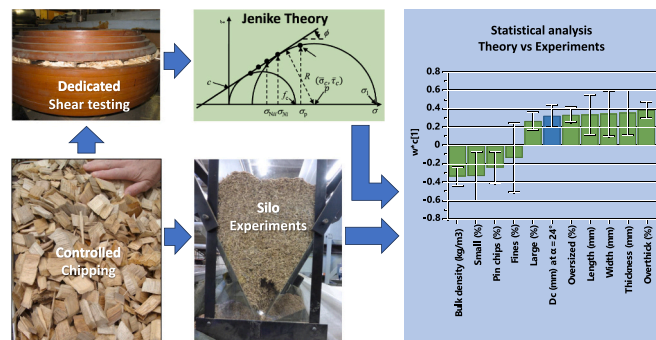
ARTICLE INFO

ABSTRACT

To achieve net-zero carbon emissions by 2050, the UK government emphasizes the pivotal role of sustainable bioenergy in electricity, transportation, and heating. However, challenges persist in handling biomass particulate solids in production facilities, leading to economic impacts. This study investigates the flow characteristics of stemwood chips from four tree species using a novel drum chipper. Experimental analyses include bulk density measurements, silo discharge studies, biomass flow property assessments, and wall friction measurements. Comparative analyses are performed using Jenike's procedure for building wedge-shaped silos, with a focus on predicting the critical opening size to prevent arching. Additionally, the paper delves into the creation of statistical models aimed at identifying key factors influencing the flow behaviour during silo discharge. Emphasis is placed on understanding potential discrepancies between theoretical predictions and experimental results concerning critical silo openings for arch-free discharge. The results contribute to understanding the factors

---

* Corresponding author at: School of Engineering, University of Greenwich, Central Avenue, Office: P154, Chatham ME4 4TB, UK.
E-mail address: H.Salehi@gre.ac.uk (H. Salehi).
[1] Present address: MoRe Research, Box 70, SE-891 22 Örnsköldsvik, Sweden.

influencing the flow behaviour of wood chips, informing silo design considerations. Our findings suggest limitations in applying traditional silo design methods, urging further research for more accurate predictions.

1. Introduction

Bioenergy applications in the heating and transportation sectors are the most cost-effective and technologically possible options to quickly reduce carbon emissions while also helping regulate rising electricity demand. The UK government's Energy Strategy illustrates that achieving net-zero carbon emissions by 2050 will necessitate the widespread use of sustainable bioenergy in electricity, transportation and heat. The contribution of bioenergy could increase by >50% between 2020 and 2026 in the UK. By 2032, sustainable bioenergy use in the UK might have increased by a ratio of 2.5, saving roughly 80 million tonnes of CO_2 equivalent in greenhouse gases. Savings like these fill the gap in emissions reductions needed to reach the country's net-zero carbon goals by 2050. Furthermore, the increased bioenergy industry sector would generate £20 billion in annual revenue and employ up to 120,000 people in the UK [1].

In the European Union, in 2014, 8200 PJ of energy were produced from renewable resources, of which 5200 PJ (approximately 63%) were obtained from biomass material, equivalent to around 196 million tonnes of oil [2]. Such production accounts for >25% of the primary energy from all sources. In Sweden, the demand for forest biomass fuels and feedstocks for energy purposes in the petrochemical and chemical industries replacing fossil feedstock was around 30 TWh/year in 2017 and is expected to rise to 45 TWh/year by 2030 [2]. Annually, more than one billion tonnes of biomass are accessible for energy needs in the United States, replacing almost one-third of US petroleum consumption [3]. A dramatic increase in the industrial use of biomass implies a demand for robust and reliable biomass bulk solids handling [4,5]. Particular concerns regarding biomass handling systems are i) wide particle size distribution, ii) high and varying moisture content, iii) low bulk density, iv) particle elasticity, and v) irregular and interlocking particles that hinder the material flow [6]. As a result, infrastructure for storing and transporting biomass that can handle this massive volume of biomass efficiently and reliably is required worldwide.

Solid biomass feedstock is composed of a wide variety of materials from different natural sources. As a first approximation, these sources can be classified into three groups: wood-derived biomasses (softwood and hardwood forestry by-products and forest-industrial residues), agricultural residues (straw, husks/shells, etc.), and wet organic waste (societal and industrial sludge, manure, etc.). Usually, these biomasses are not directly used in conversion processes, but pre-processing is necessary to obtain a more suitable form and size [7]. Wood chips are mainly used for pulp and paper production and as an energy source. Disc chippers are widely used to produce wood chips for pulp production [7]. One of the drawbacks of this chipping technology is the different cutting speeds across the disc, lower at the centre and higher at the periphery. This speed variation causes the production of fine and oversized particles, eventually reducing the yield in chemical pulping. As part of the industrial expansions, new mills with larger wood-chippers are being developed. Larger discs will increase the problem of heterogeneity due to broader speed variations throughout the disc. Drum chippers have emerged as an alternative to disc chippers, but the latter technique dominates the market [8].

In fact, due to the uniform speed across the cylindrical surface, drum chippers outweigh disc chippers, resulting in smaller contents of fines and large particles. However, the cutting angle also affects the size distribution of wood particles. The cutting angle increases the fraction of small chips, chip thickness, and bulk density. Although a lower cutting angle improves chip size homogeneity, it lowers the bulk density of the wood particles. In this study, a new type of drum chipper was used, combining the most significant features of both regular and disc

chippers. Because it is a drum chipper, there is no difference in velocity between the drum and the knife. Due to the meticulously built wood chip channels, it has the same knife-to-anvil distance and knife-to-wear-plate clearance as typical disc chippers. Compared to traditional drum chippers that produce wood particles for heat and power plants, these wood chip channels stand apart. The purpose of the channels is to direct wood particles away from the drum. The new drum chipper will only have slight differences in cutting angle. The modest difference in the cutting angle of the new drum chipper would have no discernible effect on the uniformity of the wood particles. Another critical component in producing wood particles that are uniform in size and shape is the drum size. The drum diameter should be at least ten times that of the biggest diameter of the wood logs. Smaller drum chippers produce curved wood particles of varying lengths and thicknesses [9,10]. This factor was considered while selecting logs to be chipped in this study.

Biomass material handling (storage, feeding, and transportation) is usually a problem source. The irregular and discontinuous flow of biomass material and blockage of the storage units might happen due to the mechanical interlocking of particles and bulk cohesion [6,11]. Jenike [12] developed a method to predict the minimum hopper outlet opening for conical and wedge-shaped silos. This method is a function of material bulk flow properties, hopper geometry and wall friction, and hopper inclination angle. According to Barletta and Poletto [13], the Jenike method's critical silo opening size to avoid arching for wedge shape silo estimation and the experimental results are in good agreement for wood powders. However, the Jenike method has been shown to be inadequate for designing silos for biomass materials with large/irregularly shaped particles [14,15]. Different reasons can justify these different findings on the adequacy of the Jenike method for different biomass materials. One could argue that the Jenike method's lack of predictive capability for biomass materials with large/irregularly shaped particles is because the available shear testers for measuring flow properties of particulate materials were explicitly designed for powders and relatively fine granular materials and may not be suited to coarse, and irregularly shaped particles. To address this point, a new ring shear tester, purposely built for bulk materials with large and irregular shape particles, was developed at the Wolfson Center for Bulk Solids Handling Technology at the University of Greenwich [14]. This tester is the most appropriate shear tester available to evaluate the flow properties of biomass materials in the market due to the size and the number of vanes over the lid. This shear tester was used in this research study to evaluate the flow properties of different biomass materials. To better assess the significance of the size of the shear tester and avoid the effect of the important proportions of irregularly shaped particles produced by conventional chipping procedures, the chipping procedure used in this study can produce wood chips that are all in the same size range and have no irregular forms. This study combines several novel pilot-scale concepts for material preparation and bulk property analysis. New experimental setups and procedures are adopted to determine and predict how the use of a new chipping technology affects the resulting chips' bulk flow behaviour in an industrial environment.

The overall aims of this research study were to:

I. Analyse the effects of tree species and chipper settings on the flow characteristics and the arching tendency of the resulting wood chips.
II. For each chip assortment, compare the critical silo opening size to avoid arching with the Jenike method estimates.
III. Find out, with the biomass material purposely chipped, the particle properties that are mostly responsible for affecting the

observed arching behaviour and its deviation from the Jenike theory.

2. Materials and methods

2.1. Sample preparation and sampling

Debarked logs were prepared from the four most common tree species in Sweden: Scots pine (*Pinus sylvestris*), Norway spruce (*Picea abies*), downy birch (*Betula pubescens*), and Eurasian aspen (*Populus tremula*). Aspen and birch are classified as hardwood, while pine and spruce are classified as softwood species. The logs were chipped with a novel pilot-scale drum chipper developed at Multi-Channel Sweden AB (Bredbyn, Sweden) according to procedures described by Gard Timmerfors and Jönsson [9]. The drum of the chipper was 3 m in diameter and 20 cm in width, with 16 knives that could be adjusted to control the thickness and length of the chips generated. A detailed description of the chipper, including definitions of angles and other features, has been provided by Gard Timmerfors and Jönsson [9] and Gard Timmerfors et al. [10].

In the chipping experiments, the following parameters were kept constant: circumferential drum velocity, 30 m s^{-1}, clearance/pulling angle, $\alpha = 2.2°$, and cutting/spout angle knife angle, $\varepsilon = 30°$. The knife-to-wear-plate clearance (T dimension) had two different settings: 12 and 10 mm, respectively. These settings were used to produce longer (theoretically 23–24 mm) and thicker particles (for $T = 12$ mm) and shorter (theoretically 18–19 mm) and thinner particles (for $T = 10$ mm).

Sampling was performed following SCAN-CM 41:94 by holding a 125 L polyethylene bag after the pilot chipper's 5 m long scraper conveyor. The sampling time was chosen to ensure that material from the second to the fourth log was represented. The sample amount for each assortment was approximately 80 L. The rest of the wood particles were collected for silo discharge studies.

2.2. Particle and bulk material characteristics

The average particle length, width, thickness, and mass fraction of specified size classes were measured by ScanChip image analysis as reported by Gard Timmerfors et al. [8]. The bulk density for each assortment was measured according to SS-EN ISO 17828:2016 (this work). These data were then used for modelling.

2.3. Silo discharge experimental setup

For silo discharge studies, the silo described by Barletta et al. [14] was used. It is a 0.3 m^3 bin with a wedge-shaped hopper, adjustable inclination angle, and outlet slot width (Fig. 1). For each second degree of the hopper half-angle, α, from 24° to 34°, the minimum slot width, D_c allowing complete chip discharge, was established. In each discharge experiment, the following procedures were followed: 1) the hopper inclination angle and outlet slot width were set; 2) chips were filled from the top, and the surface was levelled, with the hopper slot closed by a slab; and 3) the slab was progressively lowered with the help of a hydraulic system to allow chips to discharge. Care was given that the slab lowering was as gradual as possible in order not to disturb the material with hits or vibrations that could affect the repeatability of the test in the evaluation of the flow/no-flow limits. The procedure, therefore, is not able to provide other reliable information than the limit itself, such as solids discharge rates. Furthermore, the range of angles tested, ensures that, for all the materials, a mass flow regime is obtained and therefore, in the case of flow, the mass of residual material is negligible.

2.4. Internal friction measurements

The internal friction indicates how the bulk solid resists shear stress before it starts to flow. The internal friction of the wood chips was measured using a custom-made large ring shear tester (Fig. 2). The tester's trough has inner and outer diameters of 1 m and 0.75 m, respectively, and a depth of around 0.15 m. The 52-kilogramme open pocket lid is hung from its centre on a balancing beam [16]. The underside of the lid is flat, with pockets produced by 18 uniformly placed vertical vanes with open sides. Consolidation stress is achieved by putting deadweight on top of the lid. The tester trough rotates counterclockwise at one rev/h to shear the bulk solids material while the lid remains fixed. The stress required to maintain the lid in place is measured and reported. The test procedure is comparable to that of other ring shear testers, such as the PFT [17] and Schulze shear tester [18] and is briefly detailed below.

The shear test procedure (shown in Fig. 3) consists of a sequence of two steps: the preshearing phase (consolidation) and the shearing phase (over-consolidation). Particulate solids are sheared at normal consolidation stress (σ_c) during the preshearing stage until the shear stress approaches steady-state values. During the shearing phase, the
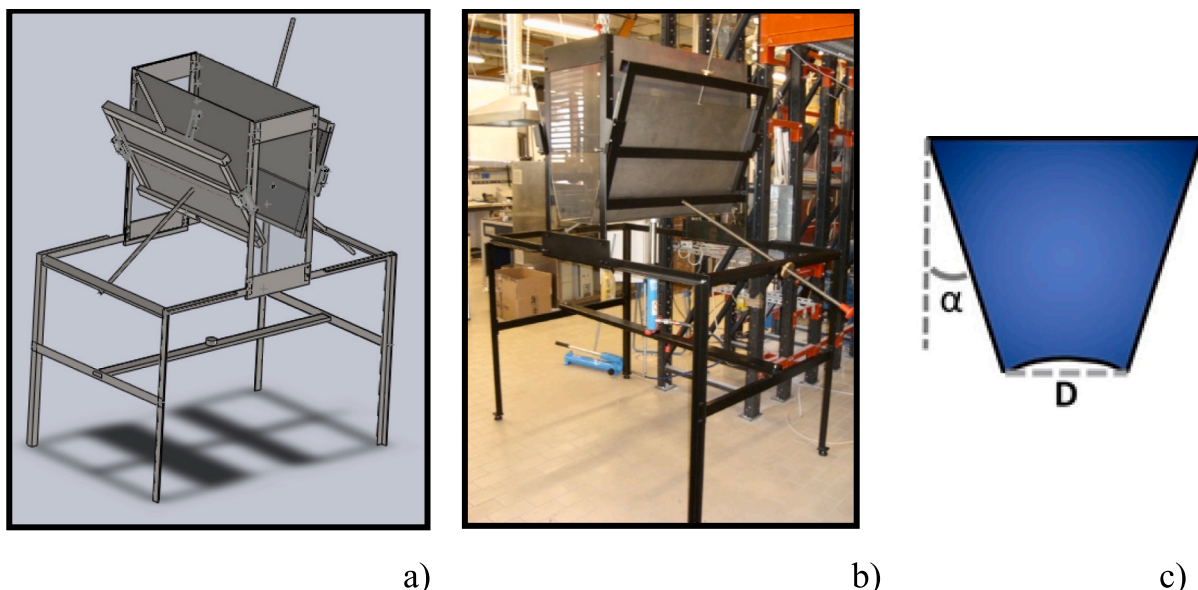

Fig. 1. a) and b): wedge-shaped hopper setup, and c): hopper half-angle, α, slot width, D.

Fig. 2. Large ring shear tester.

consolidated sample is sheared further at the lower consolidation normal stress (σ_i) until the material fails. This method is repeated with the same preshear normal stress (σ_c) but a lower shear normal stress (σ_{ii} and σ_{iii}) until a static yield loci line can be attained. The entire process for measuring material flow properties with a shear tester is provided elsewhere [16].

2.5. Wall friction measurements

A big Jenike-type tester with a shear ring (20 mm depth and 270 mm diameter) resting on a stainless-steel coupon was used to assess wall friction. The coupon steel and its surface quality are similar to the material used at the wall of the silo). The wood chips were placed in the ring and sealed with a lid. A deadweight was placed above the lid to achieve the necessary normal stress, ranging from 0.5 to 12 kPa. The shearing procedure was carried out by drawing the tester ring at a constant speed of 0.6 mm/s Using an electric pistol drill as a winch.

2.6. Yield loci, friction angle and wall friction angle calculations

Assuming linear Coulomb yield loci, each yield locus was used to evaluate experimental values of the major principal stress, σ_1, and the material unconfined yield stress, f_c. The linear regression of the shear stress data points yielded the Coulomb yield loci. The cohesiveness of bulk material, c, is defined as the material shear strength at zero normal stress. It is given by the intercept of the yield loci line with the τ axis. It is essential to emphasize that in bulk woodchips, the predominant cohesive mechanism is particle interlocking and entanglement, as opposed to

intergranular cohesive forces in conventional bulk solids. In contrast, the internal friction angle or the static angle of internal friction, ϕ, is determined by the slope of the linearised yield loci line (see Fig. 3). When c and ϕ are large, it means that particles resist flowing starting from static conditions (by rolling and sliding against one another), and the particulate has poor flow properties. The effective angle of internal friction, ϕ_e, is defined as the slope of a line that passes through both the origin of the τ and σ axis and the preshear point (σ_p, τ_p). It is a similar measure of the resistance to flow, but it is relevant to the material in motion. The effective internal friction angle defines the minimum hopper half angle to ensure a mass flow regime during silo discharge. The Major Principal Stress σ_1 during material consolidation is attained from the intersection of the σ axis with the Mohr circle representing the stress state during the preshear step (the larger one in Fig. 3). This Mohr circle passes through the preshear point (σ_p, τ_p) and is tangent to the linearised yield locus line. The strength of the bulk solids is defined by the state of stresses at the failure (shear phase) and is represented by the Mohr circle passing through the origin of the τ - σ axis and tangent to the yield locus line. The unconfined failure strength of the bulk solids f_c is estimated from the intersection of this Mohr circle with the σ axis. It is essential to emphasize that in bulk woodchips, the predominant cohesive mechanism is particle interlocking and entanglement, as opposed to intergranular cohesive forces in conventional bulk solids.

There are two different methods to draw the Mohr circle relative to the preshear, depending on the position of the preshear point. When the preshear point falls on the yield locus line or marginally above that, the method described by Nedderman [18] can be applied. According to this method, the radius, R, and the coordination of the circle's centre, p, can be calculated by Eqs. (1) and (2).

$$R = \tau_p sin\phi \tag{1}$$

$$p = \sigma_p + \tau_p tan\phi \tag{2}$$

However, in most cases, the preshear point is somewhat below the linearised yield locus. In this case, R and P can be calculated from Eqs. (3) and (4).

$$p = ctan\phi + \frac{\overline{\sigma}_c}{cos^2\phi} - \sqrt{\left(ctan\phi + \frac{\overline{\tau}_c^2}{cos^2\phi}\right)^2 - \frac{\overline{\sigma}_c^2 + \overline{\tau}_c^2}{cos^2\phi} + c^2} \tag{3}$$

$$R = \sqrt{(p - \overline{\sigma}_c)^2 + \overline{\tau}_c^2} \tag{4}$$

In both cases, the major principal stress and the unconfined failure strength can be calculated from Eqs. (5) and (6), respectively.

$$\sigma1 = p + R \tag{5}$$

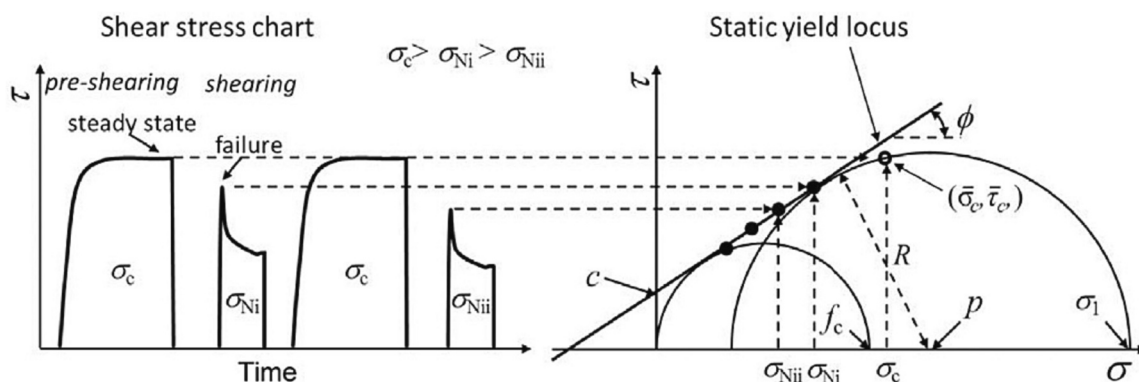$$f_c = \frac{2ccos\phi}{1 - sin\phi} \tag{6}$$

Fig. 3. Yield loci derivation from shear tester data.

These parameters are essential for the design of storage units to ensure no arch formation during material discharge.

The wall friction angle, ϕ_w, is defined as the relationship between shear and normal stress when a bulk material slides against a solid surface.

2.7. Jenike theory modelling of the critical hopper outlet size

Jenike [18] followed the hopper design procedure [17]to predict the smallest possible hopper opening size to avoid arch formation. This method builds on the hypothesis that the arch weight is held by the vertical component of the abutment stress, which is the stress within the material parallel to the arch surface close to the walls. Eq. (7) is derived from the above hypotheses on the force balance on the arch and by assuming that the formed arch is stable if the material resistance at the abutment is higher than the abutment stress, σ_1'.

$$f_c < \frac{\rho_b g D}{h(\alpha, m)} = \sigma_1' \qquad (7)$$

where f_c is the unconfined yield strength of the biomass bulk, D is the effective outlet size, ρ_b is the biomass bulk density, g is the acceleration due to gravity, $h(\alpha, m)$ is a function which takes into account the effects of variation of the thickness of the arch with the silo geometry, which depends on the hopper half-angle, α, and on the tensional state depending on the silo geometry ($m = 0$ for plane silos, $m = 1$ axisymmetric). Schulze [19] provides a graphical solution for measuring $h(\alpha)$ for different shape hoppers.

In the theory, it is assumed that the material consolidates while flowing and that the major principal consolidation stress at the silo outlet, σ_1, depends on the distance from the virtual hopper vertex. Jenike makes the hypothesis of radial stress field and stationary flow to derive Eq. (8) to estimate the major principal stress at the abutment of the arch, σ_1.

$$\sigma_1 = \rho_b g D \frac{(1 + sin\phi_e)s(m, \alpha, \phi_e, \phi_w)}{2 sin\alpha} \qquad (8)$$

where s is a complex function depending on the hopper geometry, with m and α, on the biomass effective angle of internal friction ϕ_e and wall friction ϕ_w.

The free flow criterion could be calculated from Eq. (9) by combing Eqs. (7) and (8).

$$f_c < \sigma_1' = \sigma_1 \frac{2 sin\alpha}{h(\alpha)(1 + sin\phi_e)s(m, \alpha, \phi_e, \phi_w)} = \frac{\sigma_1}{ff} \qquad (9)$$

where ff is the flow factor, calculated by Jenike and reported in diagrams for different shapes of the hopper and other values of the effective angle of internal friction of the material. On the $f_c - \sigma_1$ plane, the flow factor line (σ_1/ff) cuts the flow function curve, $FF(\sigma_1)$, which is the experimental constitutive equation of the material in which the unconfined yield stress f_c is given as a function of the consolidation stress, σ_1:

$$f_c = FF(\sigma_1) \qquad (10)$$

The intersection between the flow function and the flow factor line provides the critical unconfined yield strength of the material, f_c^*. ρ_b^* is the critical bulk density of the material at the arch. The minimum silo outlet opening size, D_c, to avoid arch formation, hence, is given by:

$$D_c = \frac{f_c^* h(\alpha)}{\rho_b^* g} \qquad (11)$$

2.8. Multivariate data analysis of particle and silo discharge properties

The multivariate analysis method Partial Least Squares Regression (PLS) was used to predict the minimum slot width, D_c, at silo discharge

for different hopper half-angles based on the material properties of the chips. PLS [20] is a strong statistical technique for modelling complex relationships between multiple independent variables and a response variable. It combines elements of principal component analysis and multiple regression to handle collinearities and noise in data effectively. PLS works by identifying latent variables, known as components, that capture the greatest variance in both the predictor variables (material properties of the chips in our case) and the response variable (minimum slot width). This simultaneous consideration of the predictor and response spaces allows PLS to identify underlying patterns and relationships in the data that might otherwise be obscured by noise.

3. Experimental results

3.1. Particle size and shape

The average size fraction of the eight chip assortments, measured with two techniques (ScanChip method and SCAN method), is reported by Gard Timmerfors et al. [7] and also reported in Table S1 in the appendix. The obtained particle thickness was higher when chipping at T 12 mm than at T 10 mm. Aspen 12 (i.e., T 12 mm) and Aspen 10 (i.e., T 10 mm) particles had the highest length, width, thickness, and fraction of over-thick particles in their respective size categories. The thickness of hardwood samples (aspen and birch) was generally higher than that of the corresponding softwood samples (pine and spruce). The hardwood assortments had more oversized and over-thick chips than softwoods. The share of fines was higher in samples chipped at $T = 10$ than at $T = 12$. The average thickness measured by the ScanChip method was somewhat lower than the thickness values given by the SCAN method. However, the average thickness value estimated by both methods shows the same tendencies, with hardwood chips being thicker than softwood chips.

3.2. Bulk density

The bulk density of the chips assortments is reported in Table 1. Bulk density is crucial in determining silo opening size to avoid arching [21]. The D_c values are inversely proportional to Bulk density; see Eq. (11). The bulk density of the tested biomass materials is close to each other and spans a narrow range, between 130 and 150 kg m^{-3}. Therefore, the change in their bulk densities was not considerably affecting the critical D_c value.

The bulk density of samples with larger particles (i.e., those chipped for average particle length 23–24 mm, such as Aspen 12, Birch 12, Pine 12 and Spruce 12) was lower than that of samples with smaller particles (i.e., those chipped for average particle length 18–19 mm, such as Aspen 10, Birch 10, Pine 10 and Spruce 10). The higher bulk density of samples chipped with the setting T 10 mm might be explained by the more significant proportion of fine particles, which can fill the voids between larger particles, thereby allowing more extra filling space. Data in Table 1 suggest that the bulk density of Birch 10 was higher than those of the other tested samples. This observation can be related to the higher density of birch wood (480–550 kg m^{-3}) compared to the other tested tree species in this study, such as quaking aspen (350–400 kg m^{-3}), Norway spruce (380–390 kg m^{-3}), and Scots pine (390–420 kg m^{-3}) [7].

3.3. Silo discharge experimental results

Fig. 4 and Table S2 reports the experimentally measured critical silo opening size, D_c, to avoid arching as a function of hopper half-angle, α, for the different chips assortments.

Generally, the critical opening size of the silo increased with the hopper half-angle, α (i.e., with decreasing wall steepness), as expected. Softwood particles were discharged at a lower critical opening size compared to hardwood particles. Spruce had a larger D_c than pine, and aspen had a larger D_c than birch. For each species, a larger D_c was

Table 1
Bulk density of the tested wood species.

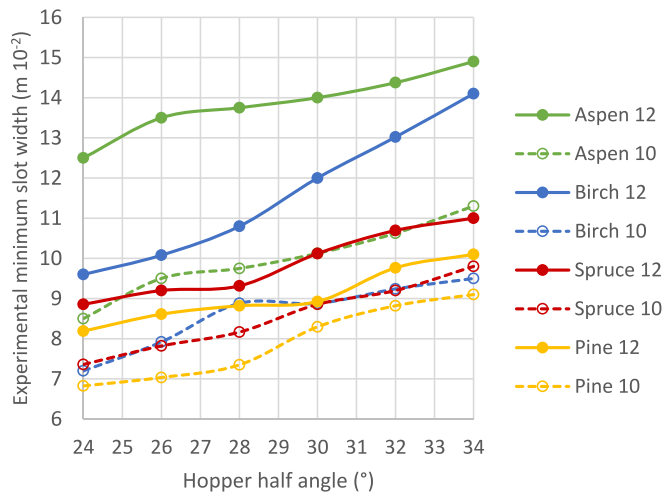|	Aspen	Aspen	Birch	Birch	Pine	Pine	Spruce	Spruce
	10	12	10	12	10	12	10	12
ρ_b (kg m^{-3})	136.3 ± 2	126.3 ± 1.7	149.4 ± 3.5	138.2 ± 3.9	145.4 ± 7.5	132.7 ± 4.5	148.5 ± 2.3	139.4 ± 1.8

Fig. 4. Experimental minimum slot width, D$_c$, vs hopper half-angle (°).

required for assortments chipped at T 12 mm than at T 10 mm, mainly due to larger particle size.

3.4. Biomass flow property measurements

The bulk material flow functions are essential because they represent how powder flowability is usually reported and classified, according to the Jenike classification [18] based on the flow factor value, $ff = \sigma_1/f_c$. The flow classes shown in Fig. 5 are generally considered for granular materials are free-flowing ($ff > 10$), easy flowing ($4 < ff \le 10$), cohesive ($2 < ff \le 4$), very cohesive ($1 < ff \le 2$), and non-flowing ($ff \le 1$). All wood chip flow functions (the unconfined yield strength as a function of the major principal stress during consolidation) results are reported in Fig. 5. The flow function of almost all wood chips in the figure falls within the cohesive region. In contrast, Spruce 10 falls on the limit between easy-flowing and cohesive ranges with an inclination towards the free-flowing area at the highest consolidation stress. The flowability of samples with larger particles is lower than the assortments with smaller particle sizes; this could correlate to the larger relative mobility of smaller particles than larger particles, resulting in lower cohesive forces and internal friction angle.

The particle size of the tested material determines a shear tester's operational range for coarse particulates. Salehi et al. [15] observed a limitation of the Schulze ring shear tester on flow property measurements of wood chips with particle sizes larger than 8 mm, owing to the lack of a defined shear plane. The Wolfson Centre Large Annular Shear Tester was used in this investigation to test flow properties (LAST).

Shearing elastic and irregular particles often result in an oscillating pattern, particularly when the shear stress reaches steady-state conditions. Salehi et al. [15] reported that, due to the interlocking ability of the tested biomaterial, shearing causes particle redistribution in the cell rather than the formation of a shear surface. A possible solution to avoid the problem is to implement a higher number of vanes in the lid, thereby preventing void formation at the back of the pocket. In this study, the wood chips had a more regular flake shape, being produced with the novel chipping method, hence we have not seen the formation of a void at the back of pockets.

The effect of moisture content on powder flow properties has been extensively studied [22,23]. We conducted sensitivity flow function experiments for Aspen 10 and 12 (dry matter of 52% ± 1 and 49% ± 1) as well as Pine 10 and 12 (dry matter of 44% ± 1 and 48 ± 1%) to investigate the effect of the added moisture content on the flow properties of the tested biomass. The dry matter of the other wood chips is presented by Timmerfors et al. [8]. The water was sprayed over the biomass bulk material at a 5% dry base. The biomass samples were adequately mixed and then covered with a plastic coverage and let stay for 1 h before their flow functions were measured with the shear tester. Samples were checked in different position to ascertain that no significant changes in moisture could be found within the sample. The flow function results, depicted in Fig. 6, showed that the added moisture slightly shifts up the flow function curves of the tested wood chips. This change did not significantly alter (P values larger than 0.2) the Jenike theory modelling of the critical hopper outlet size of the tested samples. Stasiak et al. [24] made the same observation, reporting no change in shear stress due to changing biomass moisture content. It should be emphasised that the change in the flow function of the wet-tested wood particles could be attributable to machine error rather than water addition because the difference in flow function is relatively minor.

3.5. Wall friction measurement

The traditional shear testers, such as Jenike, Brookfield PFT, and Schulze ring shear testers, cannot conduct wall friction tests due to the presence of big particles in all samples. For several biomass materials, Barletta et al. [14]found that the wall friction coefficients determined by LWFT are more significant than the wall friction angle measured by PFT, Schulze RST, and Casagrande shear box.

Fig. 7 depicts the wall friction angle results of the biomass bulk materials over stainless steel (silo wall material) for all eight assortments. Except for pine, samples with larger particles have a higher friction angle than samples with smaller particles; Pine 10 had a slightly larger wall friction angle than Pine 12. The studied hardwood samples - aspen and birch - had a somewhat lower wall friction angle than the softwood ones. With increasing applied normal stress, the wall friction angles in all samples dropped marginally.

One factor that affects the wall friction angle is the moisture content of biomass materials. Larsson [25] reported that the wall friction angle of reed canary grass is positively proportional to the samples' moisture content. We also ran a sensitivity analysis on one of the hardwood (Aspen 10) and one softwood (Pine 10) assortment to investigate if the moisture content levels (5 and 10%) affect the wall friction angle of the two biomass materials. The results showed that as the moisture content of both tested materials increased, the wall friction angle of the tested samples increased somewhat (maximum by 3%), which was consistent with Larsson's findings [25]. However, the slight change in the results was such that it did not affect the Jenike critical opening size of the hopper to avoid arching, as will be discussed in the following.

4. Discussion

4.1. Jenike discharge prediction modelling

Based on the Jenike design procedure, biomass's flow properties were used to assess the silo opening outlet size. The flow factor ff was attained from the diagrams provided by Jenike. The critical unconfined
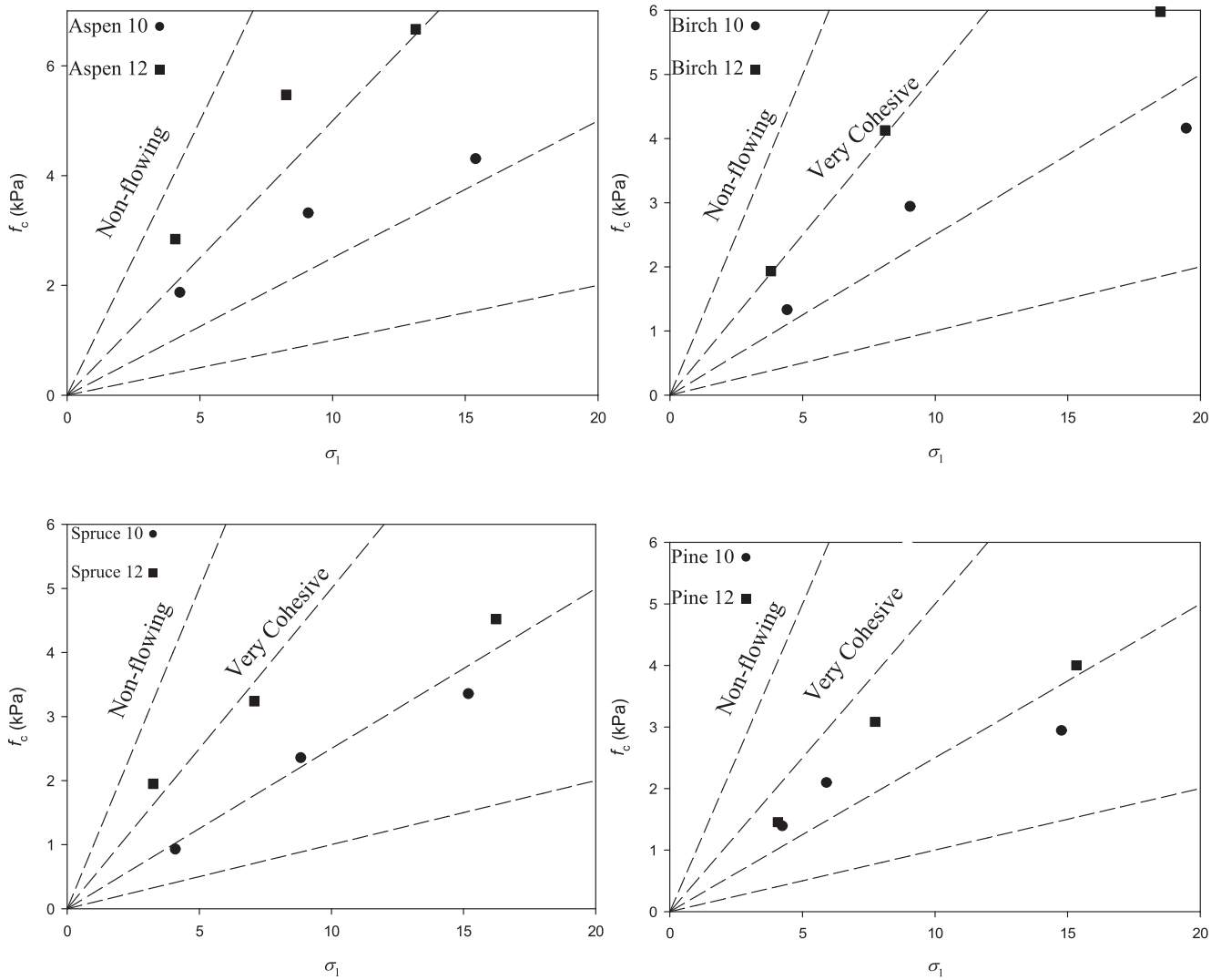
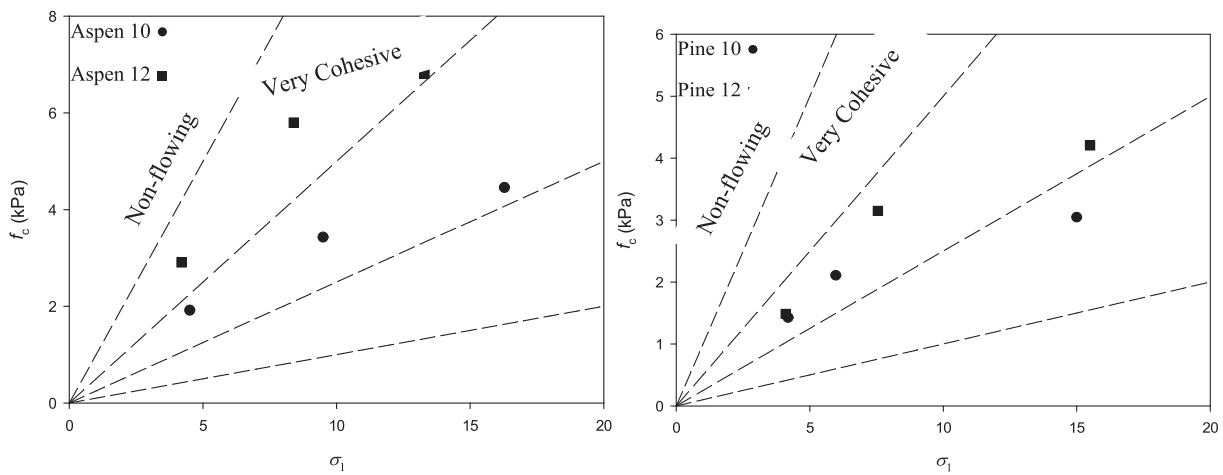Fig. 5. Biomass flow properties of different wood chips assortments.

Fig. 6. Biomass flow properties of two different wood chips assortments with added moisture.

yield strength, f_c*, and the critical bulk density, ρ_b*, were determined from the intersection between the flow function and density curves with the flow factor curve, respectively. These parameters were used in Eq. (11) to predict the critical silo opening size to avoid arch formation.

As previously mentioned Salehi et al. [15] reported that the critical opening size of the silo for the tested biomass materials was not adequately predicted by the Jenike procedure using data obtained with a Schulze ring shear tester. On the other hand, similar tests carried out
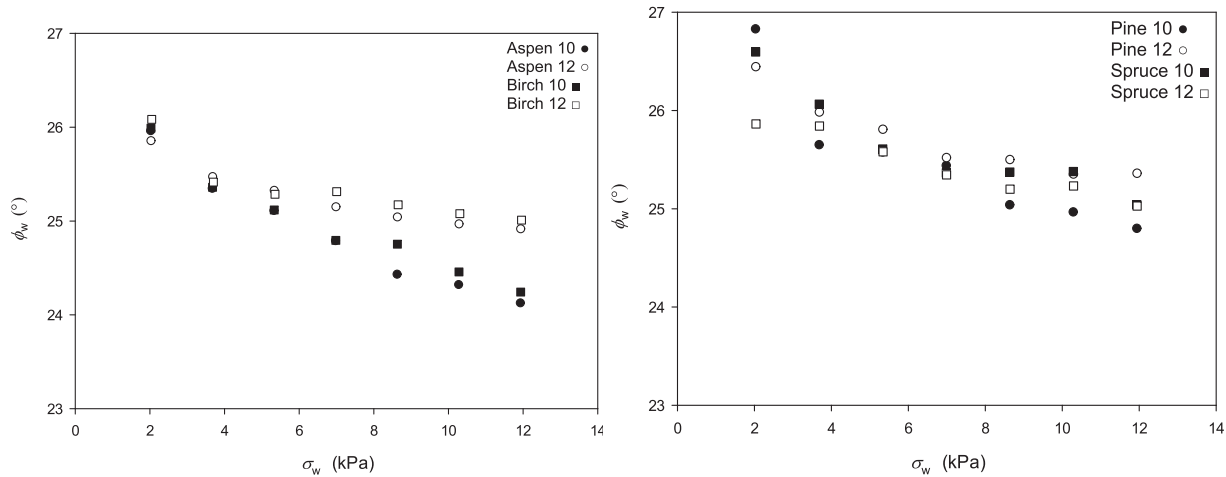
Fig. 7. Wall friction angle of the tested biomass by using a large wall friction tester (LWFT).

on wood powders showed a good agreement between Jenike theory predictions and experimentally determined critical silo openings [26]. This suggests that a possible reason may consist of the limitations of the Schulze ring shear tester in measuring the flow properties of materials with large particle sizes. However, the new ring shear tester at The Wolfson Centre can measure materials' flow properties with large particle sizes due to the large vane spacing. Fig. 8 reports the critical silo opening size to avoid arching predicted by the Jenike method using shear test data obtained with the Large Shear tester as a function of the hopper half angle.

Jenike predicted design values of the critical silo opening size, confirming the experimental trend values of D_c found in Fig. 4. However, comparing design and experimental results clearly shows that Jenike's predicted critical opening sizes for all biomass materials are conservative and significantly higher than experimental values. The big gap between the Jenike approach values and the experimental data seems to indicate a limited validity of the Jenike model for biomass silo design. Although Birch and Spruce represent distinct chip materials characterized as hard and soft, respectively, the apparent similarity in their reported values in Fig. 8 warrants further discussion. The similarity in reported values for Birch12 and Spruce12 may be attributed to various factors, including the inherent variability in material properties, and the

limitations of the Jenike model. Despite their classification as hard and soft chips, the specific frictional and mechanical and particle size characteristics of Birch12 and Spruce12 might lead to comparable flow behaviors in the tested conditions. It's crucial to note that the complexities of biomass materials can sometimes result in unexpected similarities in flow properties despite apparent differences in hardness.

Material bulk cohesion, c, is an essential factor in silo design by using the Jenike method. However, it is speculated that biomass bulk cohesion, c, is not considered the primary mechanism in the stabilising arch. Long-distance interaction in the material due to fibres might connect the arch material to the upper layer inside the silo where higher local stresses occur, and the stability of the arch could instead be attributed to tensile strength than to unconfined yield strength. In addition, Owoni-koko et al. [11] argued that due to the bulk solid's mechanical interlocking, the bulk solid's tensile strength is a more relevant flow property than the compressive strength. This is true when we have irregularly shaped particles. The wood particles produced from the introduced novel chipping method have regular flake shape particles; hence we have not seen the mechanical interlocking of the particles.

To quantify the relationship between Jenike prediction values and the critical silo opening size of the tested biomass materials, the Jenike estimated values were regressed over the experimental results. The coefficient of this regression, calculated by minimising the sum of squared errors, is interpreted as the safety factor of Jenike predictions. This safety factor is 0.323, and the R^2 value of the regression model is 0.97, which indicates a very good fit. This simple regression model could be developed further to the two-level categorical regression model. This model considers the tree species and the chipping knife angle as the categorical variables. The model could be used to understand better these variables' effects on the relationship between the Jenike model and experimental results. The estimated intercept values of the developed categorical regression model are presented in Table 2.

The estimated intercepts in Table 2 indicate the values that should be added to the Jenike model's overestimation based on the type of trees and chipping knife angle. This intercept is maximum for Birch10 (5.15) and minimum for Spruce12 (3.20). The Jenike coefficient in two-level categorical regression is 0.191, which is lower than the safety factor estimated by the regression model, 0.323. This is due to considering intercept in the two-level categorical model, which decreases the model's coefficient value.

4.2. Multivariate modelling of silo discharge behaviour

One could claim that the elasticity of biomass materials caused situations in which stress from the upper part of the silo was not transmitted to the lower half of the silo. This may have resulted in a lower D_c
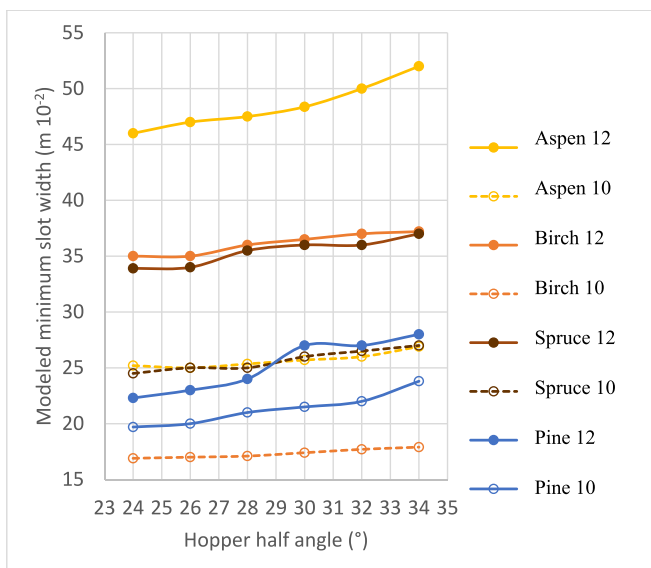

Fig. 8. Modelled minimum slot width vs hopper half angle.

experimental value, but the Jenike design approach does not account for this effect in the silo design. Furthermore, the disparity between the observed and model results could be attributed to the small size of the experimental silo rig compared to massive industrial storage units. Even though the critical opening size for mass flow discharge of the Jenike approach is independent of the silo/hopper size, this argument could be correct. Jenike assumed that all particle materials inside the silo had attained a critical steady-state shear condition, in which neither the shear stress nor the material bulk density changed unless the normal consolidation stress changed. However, using the tested fibrous biomass material, the needed travel distance to reach the hopper outlet in the tested rig may not be sufficient to establish steady conditions. This means that the material in the silo could be under-consolidated and, therefore justify weaker materials and smaller experimental critical arching. This hypothesis may be supported by the difference between experimental results and Jenike estimates that tends to decrease slightly with larger hopper opening sizes. In this condition, higher biomass consolidation stress is achieved. Thus it is less sensitive to attaining the steady state (critical) condition. Most industrial process operations are the same size as the tested rig utilised in this study. However, to apply this study's findings to bigger storage units, additional research using a larger-scale silo is required, and this has been scheduled as a follow-up project.

To identify the characteristics of the particulates mostly affecting the critical arching size, we used partial least squares regression (PLS) to compare responses and multiple explanatory variables. This method [20] is similar to main components regression, but creates a linear regression model by projecting the predicted and observed variables to a new space instead of identifying hyperplanes of maximum variance between the response and independent variables. A simple PLS model with one component could be created to predict the D_c at $\alpha = 24°$ with $R^2 = 0.81$ and $Q^2 = 0.75$.

The R^2 number defines the goodness of fit for the given model. The R^2 is a fraction number from zero to one, indicating how much of the overall variation in the response variable is captured by the fitted model. Numbers around zero suggest that the model did not capture the variations in the response variable; values near one indicate that the fitted model caught substantially all of the variability. The R^2 is determined using Eq. (12), where $\widehat{Y}$ is the estimated value for the response variable, y_i is the observed response variable, and $\bar{y}$ is the average of the response variable.

$$R^2 = 1 - \frac{\sum\limits_{i=1}^{n}(y_i - \widehat{Y}_i)^2}{\sum\limits_{i=1}^{n}(y_i - \widehat{Y}_i)^2 + \sum\limits_{i=1}^{n}(\bar{y}_i - \widehat{Y}_i)^2} \quad (12)$$

The model's prediction accuracy is represented by the Coefficient of Multiple Determination (Q^2), which is obtained using Eq. (13). Q^2 is a value between zero and one that indicates how much of the response variable's variance can be predicted by the model. Q^2 is defined similarly to R^2, but in the Coefficient of Multiple Determination, errors are estimated based on the difference between experimental outcomes (y) and projected values ($\widehat{P}$). This criterion aims to determine how much the expected values differ from the observed values. As with R^2, larger values indicate that the constructed model has superior predictive capacity.

$$Q^2 = 1 - \frac{\sum\limits_{i=1}^{n}(y_i - \widehat{P}_i)^2}{\sum\limits_{i=1}^{n}(y_i - \widehat{P}_i)^2 + \sum\limits_{i=1}^{n}(\bar{y} - \widehat{P}_i)^2} \quad (13)$$

The scatter and loading plots in Fig. 9a and b are interpreted by looking at how the individual samples (9a) correspond to the measured material properties (9b). Each bar in score plot (9a) represents a specific sample, and its absolute value is the deviation from the mean value of all measured properties. Each bar in the loading plot (9b) is the coefficient of a measured property; absolute value corresponds to the explanatory power of that property for the prediction model. The positions of the sample and property bars show positive and negative correlations between samples and properties. Hence, in 9a, it is revealed that Aspen 12, an extreme to the right, corresponds to a high percentage of over-thick chips and a low bulk density (extreme properties in 9b). The opposite is true for Spruce 10, furthest to the left in 9a, having a high bulk density and a low percentage of over-thick chips. By only studying 9b, one can see that an assortment with a percentage of over-thick chips probably has a low bulk density.

The predicted response in the PLS model was D_c, and is assigned with a positive value and a different colour (blue) in Fig. 9b. The positive correlation with the modelled coefficients for the percentage of over-thick and oversized particles and average values for thickness, width, and length, reveals that high values for these factors increase the size of D_c. On the contrary, high values for negatively correlated coefficients (bulk density and percentage of small and pin chips) decrease the D_c. Figure 9c illustrates the model's predicted vs. observed values for D_c.

These findings tend to support the hypothesis made in section 5.1 above, that the discrepancies between the Jenike theory and the experiments in the case of biomass, could be attributed to the difficulty of this material to reach the steady state in the silo and, therefore, reach the outlet under low consolidation state that is responsible for the increased material flowability than predicted from shear tests.

5. Conclusions

Literature indicates that Jenike's theory for silo arching has different suitability for different kinds of biomass. It works well with sawdust but is largely conservative for biomass with larger particle sizes. The use of a new drum chipper allowed obtaining regularly shaped wood chips from 4 different wood species that allowed the assessment of the role of particle size only without the effect of particle shape. The arching behaviour of these biomass samples was studied in a wedge-shaped hopper. Measurements were taken at various hopper half angles and opening widths to determine the critical opening size resulting in a stable arch formation. To analyse the flow functions of wood particulates with large particles, a new shear tester developed at the University of Greenwich was used. The design values of the crucial opening size produced by the Jenike technique for silo design were larger than the experimentally determined values. The safety factor of the Jenike approach is 0.323. This factor was estimated by comparing Jenike approach estimates and the experimental results. In addition, a two-level categorical regression model was developed based on experimental results.

The feedstock factors that significantly impacted the difference between the experimental silo discharge tests and the Jenike model values for the minimum slot width at a 28° hopper half-angle were identified using multivariate partial least square modelling. Particle length and thickness were the most critical feedstock parameters for predicting the Jenike model's overestimated minimum slot width. Both factors had a positive influence and provide a model with a good coefficient of determination and a statistically significant p-value. This model was used to understand the impact of different tree species better and chipping settings for different particle lengths on critical opening size to avoid arching. The majority of the findings indicate that the lower
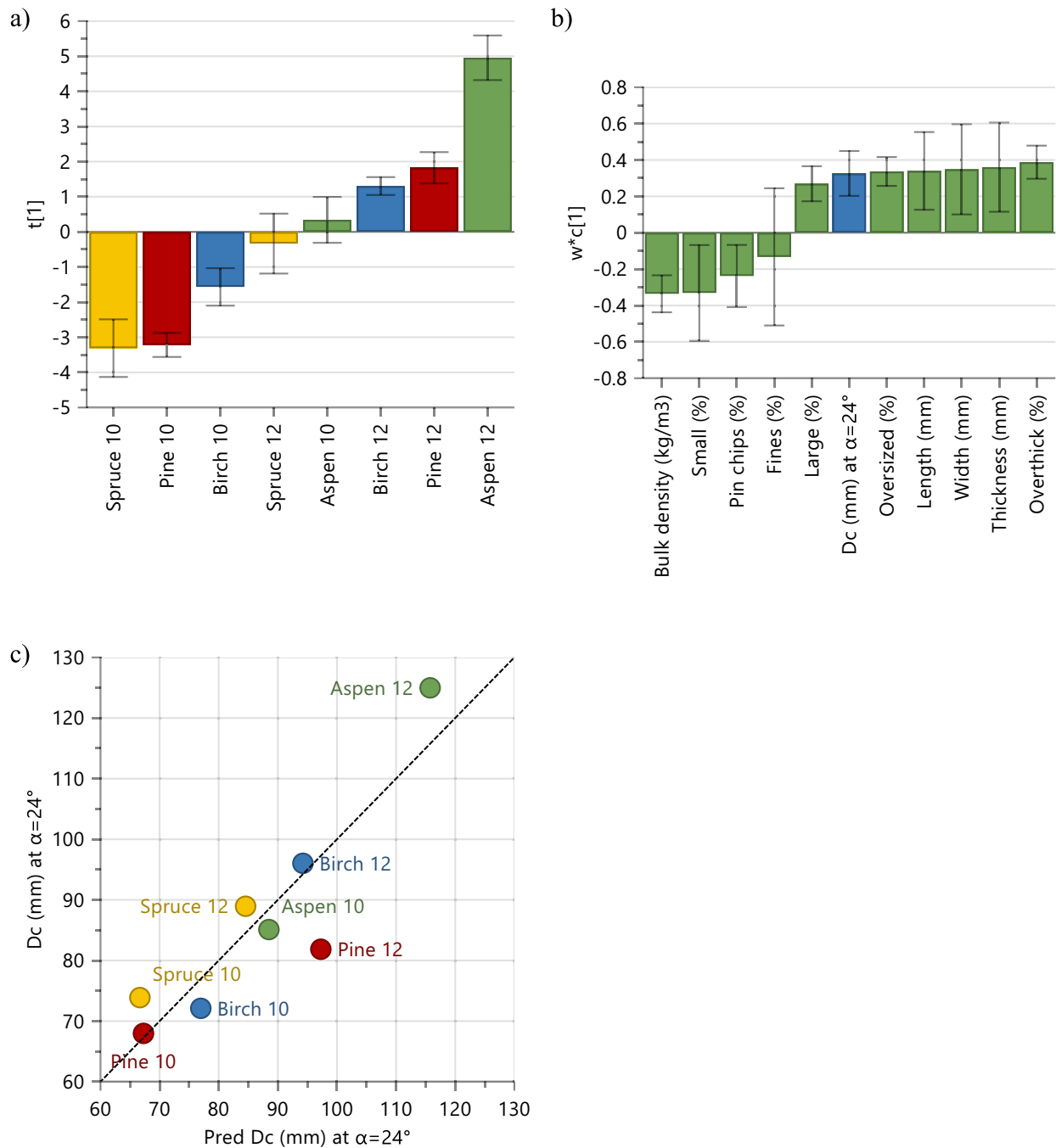
Table 2
Two-level categorical regression intercepts.

Wood species	T 10 mm	T 12 mm
Birch	5.15	4.84
Aspen	4.95	4.64
Pine	4.18	3.87
Spruce	3.51	3.20

Fig. 9. PLS prediction model of D$_c$ (mm) at α = 24°. a) Scatter plot of the assortments' deviation from the mean value of all measured properties, b) Loading plot of the modelled coefficients of the assortment's properties, c) Observed vs Predicted D$_c$ values (R2 = 0.81, Q2 = 0.75). The bars in a) and c) are coloured by species. The blue bar in b) is coloured differently than the other bars to emphasize that it is the predicted response. Error bars in a) and b) show 95% confidence intervals from the mean, obtained by leave-one-out cross-validation. (For interpretation of the references to colour in this figure legend, the reader is referred to the web version of this article.)

critical outlet size observed in silo experiments is attributed to the under-consolidation of the material at the outlet. This under-consolidation is a result of the longer travel distances required for these materials to attain a steady state.

CRediT authorship contribution statement

Declaration of Competing Interest

The authors declare that they have no known competing financial interests or personal relationships that could have appeared to influence the work reported in this paper.

Data availability

Data will be made available on request.

Acknowledgements

Appendix A. Supplementary data

Supplementary data to this article can be found online at https://doi.org/10.1016/j.powtec.2023.119174.

References

[1] REA, REA Bioenergy Strategy Phase 3: Delivering the UK's Bioenergy Potential, 2019.
[2] European Environmental Agency, Renewable Energy in Europe — Recent Growth and Knock-on Effects, 2016.
[3] V. Balan, Current challenges in commercially producing biofuels from lignocellulosic biomass, ISRN Biotechnol. 2014 (2014) 1–31, https://doi.org/10.1155/2014/463074.
[4] D. Barletta, M. Poletto, An assessment on Silo design procedures for granular Woody biomass, Chem. Eng. Trans. 32 (2013) 2209–2214, https://doi.org/10.3303/CET1332369.
[5] T.A. Lestander, B. Johnsson, M. Grothage, NIR techniques create added values for the pellet and biofuel industry, Bioresour. Technol. 100 (2009) 1589–1594, https://doi.org/10.1016/j.biortech.2008.08.001.
[6] Á. Ramírez-Gómez, Research needs on biomass characterization to prevent handling problems and hazards in industry, Part. Sci. Technol. 34 (2016) 432–441, https://doi.org/10.1080/02726351.2016.1138262.
[7] M. Ek, G. Gellerstedt, G. Henriksson, Wood Chemistry and Wood Biotechnology, 2009.
[8] J.G. Timmerfors, H. Salehi, S.H. Larsson, T. Sjölund, L.J. Jönsson, The impact of using different wood qualities and wood species on chips produced using a novel type of pilot drum chipper, Nord Pulp Paper Res J. 36 (2021), https://doi.org/10.1515/npprj-2019-0096.
[9] J.G. Timmerfors, L.J. Jönsson, Evaluation of novel drum chipper technology: pilot-scale production of short wood chips, TAPPI J. (2019), https://doi.org/10.32964/tj18.10.585.
[10] J. Gard Timmerfors, T. Sjölund, L.J. Jönsson, New Drum-Chipping Technology for a More Uniform Size Distribution of Wood Chips, Holzforschung, 2020, https://doi.org/10.1515/hf-2018-0279.
[11] A. Owonikoko, R.J. Berry, M.S.A. Bradley, The difficulties of handling biomass and waste: characterisation of extreme shape materials, Bulk Solids Handling. 31 (2011).
[12] A.W. Jenike, Gravity flow of solids, Trans. Inst. Chem. Eng. 40 (1962) 264.
[13] D. Barletta, M. Poletto, An Assessment on Silo Design Procedures for Granular Woody Biomass, 2013, https://doi.org/10.3303/CET1332369.
[14] D. Barletta, R.J. Berry, S.H. Larsson, T.A. Lestander, M. Poletto, Á. Ramírez-Gómez, Assessment on bulk solids best practice techniques for flow characterization and storage/handling equipment design for biomass materials of different classes, Fuel Process. Technol. 138 (2015) 540–554, https://doi.org/10.1016/j.fuproc.2015.06.034.
[15] H. Salehi, M. Poletto, D. Barletta, S.H. Larsson, Predicting the silo discharge behavior of wood chips - a choice of method, Biomass Bioenergy 120 (2019) 211–218, https://doi.org/10.1016/j.biombioe.2018.11.023.
[16] H. Salehi, D. Barletta, M. Poletto, A comparison between powder flow property testers, Particuology. 32 (2017) 10–20, https://doi.org/10.1016/j.partic.2016.08.003.
[17] R. Berry, M. Bradley, R. McGregor, Brookfield powder flow tester - results of round robin tests with CRM-116 limestone powder, in: Proceedings of the Institution of Mechanical Engineers, Part E: Journal of Process Mechanical Engineering 229, 2014, pp. 215–230, https://doi.org/10.1177/0954408914525387.
[18] R.M. Nedderman, Statics and Kinematics of Granular Materials, Cambridge University Press, 1992.
[19] D. Schulze, Powders and Bulk Solids, Springer Berlin Heidelberg, Berlin, Heidelberg, 2008, https://doi.org/10.1007/978-3-540-73768-1.
[20] H. Latan, R. Noonan, Partial Least Squares Path Modeling: Basic Concepts, Methodological Issues and Applications, Springer International Publishing, 2017, https://doi.org/10.1007/978-3-319-64069-3.
[21] H. Salehi, R. Berry, R. Farnish, M. Bradley, Temperature and time consolidation effect on the bulk flow properties and arching tendency of a detergent powder, Chem. Eng. Technol. 43 (2020) 150–156, https://doi.org/10.1002/ceat.201900092.
[22] G. Landi, D. Barletta, M. Poletto, Modelling and experiments on the effect of air humidity on the flow properties of glass powders, Powder Technol. 207 (2011) 437–443, https://doi.org/10.1016/j.powtec.2010.11.033.
[23] H. Salehi, V. Karde, H. Hajmohammadi, S. Dissanayake, S.H. Larsson, J.Y.Y. Heng, M. Bradley, Understanding flow properties of mannitol powder at a range of temperature and humidity, Int. J. Pharm. 596 (2021), 120244, https://doi.org/10.1016/j.ijpharm.2021.120244.
[24] M. Stasiak, M. Molenda, M. Ba Da, E. Gondek, Mechanical properties of sawdust and woodchips, Fuel. 159 (2015) 900–908, https://doi.org/10.1016/j.fuel.2015.07.044.
[25] S.H. Larsson, Kinematic wall friction properties of reed canary grass powder at high and low normal stresses, Powder Technol. 198 (2010) 108–113, https://doi.org/10.1016/j.powtec.2009.10.022.
[26] D. Barletta, M. Poletto, An Assessment on Silo Design Procedures for Granular Woody Biomass, 2013, https://doi.org/10.3303/CET1332369.